Solar Energy 153 (2017) 718–731

Contents lists available at ScienceDirect

Solar Energy

journal homepage: www.elsevier.com/locate/solener

Optimal passage size for solar collector microchannel and tube-on-plate absorbers

R.W. Moss [a,*], G.S.F. Shire [a], P. Henshall [b], P.C. Eames [c], F. Arya [d], T. Hyde [d]

[a] School of Engineering, University of Warwick, UK
[b] Science and Technology Facilities Council, formerly Centre for Renewable Energy Systems Technology, Loughborough University, UK
[c] Centre for Renewable Energy Systems Technology, Loughborough University, UK
[d] School of the Built Environment, University of Ulster, UK

ARTICLE INFO

Article history:
Received 26 January 2017
Received in revised form 5 April 2017
Accepted 9 May 2017

Keywords:
Solar collector
Solar absorber
Single pass
Double pass
Thermal
Flat panel
Heat transfer
Laminar
Turbulent
Microchannel
Serpentine
Pressure drop
Pumping power
Optimisation

ABSTRACT

Solar thermal collectors for buildings use a heat transfer fluid passing through heat exchange channels in the absorber. Flat plate absorbers may pass the fluid through a tube bonded to a thermally conducting plate or achieve lower thermal resistance and pressure drop by using a flooded panel or microchannel design. The pressure drop should be low to minimise power input to the circulating pump.

A method is presented for choosing the optimum channel hydraulic diameter subject to geometric similarity and pumping power constraints; this is an important preliminary design choice for any solar collector designer. The choice of pumping power is also illustrated in terms of relative energy source costs.

Both microchannel and serpentine tube systems have an optimum passage diameter, albeit for different reasons. Double-pass and flooded panel designs are considered as special microchannel cases. To maintain efficiency, the pumping power per unit area must rise as the passage length increases. Beyond the optimum pumping power the rise in operating cost outweighs the increase in collector efficiency.

1. Introduction

Solar thermal collectors generally extract heat to a fluid that passes through a tube bonded to the absorber plate, passages embedded inside the plate or a flooded panel.

For a given absorber area, the designer must select the tube diameter and length and choose between a single pipe or a microchannel arrangement with multiple passages. High heat transfer coefficients can be obtained using small-bore pipe but will incur high frictional losses and increase the power required to circulate the fluid. The pumping power contributes to the operational cost and should be minimised where possible: an optimum solar collector design will achieve the highest possible efficiency at its target pumping power.

This paper describes a methodology for choosing the optimum channel size for a given solar collector plate area in terms of the allowable pumping power and fluid properties.

Previous work within our group (Oyinlola et al., 2015a, 2015b) has experimentally investigated the validity of Nusselt number correlations for laminar flow microchannel plates with various channel depths and flow rates. Oyinlola et al. (2015c) studied conjugate heat transfer effects due to conduction along the microchannel plate.

Regardless of the configuration or working fluid there is always an optimum size for the coolant channels, this being the hydraulic diameter that for a given operational cost (pumping power) will keep the mean fluid temperature closest to the fluid inlet and minimise unnecessary heat losses to the environment. The choice of channel or pipe diameter may ultimately be influenced by additional factors such as available material dimensions or ease of manufacture but a designer should always calculate the optimum

* Corresponding author.
E-mail address: r.moss@warwick.ac.uk (R.W. Moss).

http://dx.doi.org/10.1016/j.solener.2017.05.030
0038-092X/

Nomenclature

a, b	rectangular channel width and depth
A_c	collector top surface area
A_h	internal surface area for heat transfer (sum over all channels)
c	fluid specific heat capacity
D_h	channel hydraulic diameter
f	Fanning friction factor
F	fin efficiency parameter
F'	collector efficiency factor
F''	collector flow factor
F_P	passage efficiency factor
F_R	collector heat removal factor
G	total (beam & diffuse) irradiance from Sun
H	plate height (m)
h	heat transfer coefficient inside a channel
k	fluid thermal conductivity
k_m	metal thermal conductivity
L	length of a tube or passage (m)
$\dot{m}$	coolant mass flow rate (kg/s)
m^*	dimensionless collector mass flow rate
n, N	number of flow passages (actual, equivalent)
Nu_H	Nusselt number for laminar flow, constant heat flux boundary
p, P	passage pitch (actual, equivalent)
Po	Poiseuille number, $f = \frac{\text{Po}}{\text{Re}}$
$\dot{Q}$	volume flow rate (m^3/s)
Q_u	rate of heat extraction by fluid
r, R	void fraction (actual, equivalent)
Re	Reynolds number
S^*	net solar power absorbed by the collector after heat losses
s	channel aspect ratio
$T(x)$	double-pass metal temperature distribution
T_a	ambient temperature
T_i	fluid temperature at inlet to collector
T_o	fluid temperature at outlet from collector
T_{pm}	collector plate mean temperature
U_L	overall collector heat loss coefficient
v	fluid velocity in channels
W_p	fluid pumping power per m^2 top surface area
W_{TOT}	total pumping power (W)
W	plate width (m)
η	collector efficiency
θ	fluid temperature rise along channel
μ	fluid dynamic viscosity
ρ	fluid density
$\tau\alpha$	effective transmissivity-absorbance product
ΔP	fluid pressure drop along each channel
ΔT_h	metal to fluid temperature difference
$\Delta T, \bar{T}$	difference between mean plate surface and fluid inlet temperatures

size and, if they adopt a different dimension, assess its performance implications.

The choice of pumping power is a separate question but is considered here briefly to show typical values and illustrate how they are determined.

This work was initiated as part of the design and testing of a vacuum-insulated flat plate collector (Henshall et al., 2016). The initial absorber concept used a microchannel plate. The optimum hydraulic diameter was however found to be of order 2 mm, which allowed a change in design to a flooded panel made from hydroformed sheets. The application of the proposed technique is much wider than the solar collector field, with or without vacuum insulation, since the same considerations will apply to any heat exchanger subject to a constant rate of heat input. The particular interest for solar collectors, which can never be perfectly insulated from their environment, is to improve the heat collection efficiency by minimising heat losses. Other applications may have different targets, for instance concentrating PV systems may use a microchannel cooling system to improve the PV efficiency (Radwan et al., 2016).

Many previous workers have studied the optimisation of flat panel collectors (Bracamonte and Baritto, 2013; Eisenmann et al., 2004; Chen et al., 2012; Do Ango et al., 2013; Roberts, 2013). Sharma and Diaz (2011) recognised that the optimal microchannel dimensions are a compromise between heat transfer and pressure drop. Farahat et al. (2009) calculated the exergy efficiency of a flat plate collector as a function of pipe diameter and flow rate. Hegazy (1996, 1999) calculated the optimum channel depth, to maximise heat gain for a given pumping power, for turbulent flow in a solar air heater; the present work reaches an equivalent result for laminar flow of a fluid. Mansour (2013) built a mini-channel plate with 2 mm × 2 mm square channels to maximise thermal performance with reasonable power consumption for the pump but did not prove that his channel size was optimal. Cerón et al. (2015) performed a highly detailed 3D numerical simulation of the air convection within a flat panel enclosure and the water inside its serpentine tube absorber. Visa et al. (2015) recognised that large pressure drops would occur if the tube diameter were too low. He built absorbers with three different combinations of tube diameter and length to determine the optimum via experimental measurements; no justification was given for the chosen sizes. Notton et al. (2014) tested a solar-absorbing gutter and ran a detailed simulation of possible improvements. They noted the importance of the electrical power required for pumping; their pump consumed between 30 and 250 W (for 1.8 m^2 panel), depending on the flow rate. Nano-fluids have been used to enhance the heat transfer or reduce the pumping power (Colangelo et al., 2015; Hussien et al., 2016).

Additional factors affect hybrid PV/T collectors since they suffer reduced electrical efficiency at high temperatures: there is an optimum temperature that maximises exergy efficiency (Evola and Marletta, 2014). Agrawal and Tiwari (2011) investigated the effect of various microchannel depths in optimising the exergy efficiency of air-cooled PVT modules.

2. Optimum pumping power

A designer should ideally choose how much pumping power is necessary for circulating the fluid and then identify an optimum combination of channel diameter and flow rate subject to this constraint. This is a better approach to panel design than setting a fixed flow rate since it separates any system optimisation into two separate parts: choice of pumping power (dependent on system economics) and design of the most efficient solar panel for a given pumping power.

The choice of pumping power will depend on many factors. The pump could be powered by mains electricity, in which case the electricity cost is a factor, or one could add a small PV panel driving a high-efficiency pump (Caffell, 1998). Dubey and Tiwari (2009)

simulated the performance of a system using 0.165 m^2 of PV panel (covering part of the thermal collector area) to drive a 35 W circulating pump for 2 m^2 of water heating panels; their pumping power was 17.5 W/m^2. A number of authors (Farahat et al., 2009; Aste et al., 2012; Evola and Marletta, 2014; Nikoofard et al., 2014) have covered the techno-economic and exergetic optimisation of solar thermal collectors in more depth than is possible here.

For completeness however the following example illustrates the possible optimisation of a variety of systems subject to some cost penalty associated with the use of electricity.

Table 1 defines a water heating system using a pair of typical, tube on plate, thermal collectors that may be connected either in series or parallel. The values were chosen for illustration purposes and are not based on any experimental system. Collector efficiency has been predicted using the methods described in Sections 3 and 4 below.

A third simulation modelled the same pump and pipework connected to a microchannel collector with 6 mm × 6 mm square passages.

Any optimisation process must define the electrical cost of the pumping power. There are two very similar kinds of target:

- if the solar collector does not generate sufficient heat (so some gas must be burnt to meet the short-fall) the question is to minimise the cost of gas + electricity (whether financial or in terms of carbon emissions) for the required thermal output.
- conversely an off-grid system might use a PV panel covering part of the thermal collector (as Dubey and Tiwari, 2009) to drive the pump; the target then is simply to maximise the heat collected. Note that if the thermal and PV panels do not overlap, the solution would be to add the largest possible PV panel. It is then not an optimisation problem.

The latter option was chosen for this example. There are two competing effects: using a larger fraction of the available area for PV reduces the area available to collect heat but increases the efficiency of the thermal collector (Fig. 1).

The "Constant η" line shows the effect due to shading of part of the thermal panel area; the change in output *relative to* this line is due to the drop in collector efficiency at high $T_{pm} - T_i$. Whilst the thermal benefit is relatively small, the improvement due to an optimised design may be possible without any additional cost. The effects of transition are evident in the Reynolds number range 2000–3000 (assumed linear between laminar and turbulent). At high pumping powers (e.g. 40 W) the effective heat output for the serpentine tube panels has fallen by approximately 6% from its peak value due to the shading of the thermal panel by the required PV area.

Table 1
System parameters for optimisation example with tube-on-plate collectors.

Total thermal panel area	4 m^2 (two panels, each 2 m long × 1 m wide)
Tube internal diameter	0.01 m
Tube pitch	0.0667 m (15 m pipe per m^2 of collector, $R = 0.15$)
Plate material	1050 aluminium, 0.9 mm thick
Coolant	Tyfocor LS
Ambient temperature	30 °C
Coolant inlet temperature to panel T_i	70 °C
Irradiance (perpendicular to panel) G	1000 W/m^2
Transmission-absorbance product $\tau\alpha$	0.87
Heat loss coefficient U_L	3.8 W/m^2 K
PV panel efficiency	0.2
External pipework (for total pressure drop)	Equivalent to 30 m length of 0.02 m bore pipe
Pump efficiency	0.5

Table 2 lists the optimum points for these systems. At higher pumping powers there is only a small potential for increased collector efficiency but a severe drop in output, due to the difference in efficiency between the thermal and PV panels, as the PV panel area increases.

Connecting the pair of serpentine tube absorbers in parallel rather than series raises the heat output by 1.4% due to the reduced pressure drop and increased flow rate. The microchannel plate achieves a further 1.4% gain. This is probably insufficient to justify the higher manufacturing costs of a microchannel absorber unless such a design could be cheaply fabricated in extruded or injection-moulded plastic (Do Ango et al., 2013).

Using a 4 mm thick plate made of high density polythene ($k = 0.52$ W/m K) would for instance reduce the serpentine plate overall efficiency to 0.57. The microchannel plate efficiency would only fall slightly, to 0.695, because the microchannel concept achieves a much shorter conduction path length.

A similar analysis for a grid-connected system using mains electricity instead of a PV panel might be subject to a condition $\frac{\text{Cost of electricity (£/kW h)}}{\text{Cost of gas (£/kW h)}} = 3.2$ i.e. slightly less severe than the PV-powered $\frac{\eta_{TH}}{\eta_{PV}} \approx 3.5$. The optimum conditions are very similar to the PV case: mass flows increase by 3–5% and total pumping power increases by 9–13%.

These results for a conceptual system indicate that the optimum power lies in the range 0.01–1.6 W/m^2 for panels covering 4 m^2. The dimensions chosen are close to optimal for the microchannel system: the optimal size for the parallel and series configurations will be discussed in Section 4.

Sections 3 and 4 below show that heat removal factor is a function of panel area as well as pumping power (W/m^2) and suggest scaling laws for the necessary increase in pumping power to maintain efficiency as panel dimensions are increased. The optimisation results will vary depending on the actual system configuration and optimisation criteria.

3. Thermo-fluid analysis of microchannel absorbers

3.1. Introduction

Flat plate solar collectors usually rely upon the flow of a water-based coolant to extract heat from the absorber; the alternative using heat pipes (Deng et al., 2013; Xu et al., 2015) is not considered here. The coolant may pass along a tube bonded to the plate, Fig. 2(a); through multiple parallel microchannels, Fig. 2(b); or within a flooded panel, Fig. 2(c). "Microchannel" will be used here to identify any arrangement having parallel passages, without implying any size limit, passage shape or manufacturing method.

Two analysis methods will be described. The first provides an analytical solution for optimum passage size in microchannel systems: the flow is laminar and material conductivity high enough to have little effect on the result. The second technique uses numerical modelling to determine the optimum size even in serpentine tube systems with turbulent flow, bend losses and more significant conduction effects.

The efficiency of a flat plate solar collector is commonly defined in terms of a heat loss coefficient U_L and the mean plate surface temperature T_{pm} (Duffie and Beckman, 2013):

$$\eta = \frac{Q_u}{A_c G} = \left[(\tau\alpha) - \frac{U_L(T_{pm} - T_a)}{G}\right]$$

Efforts to maximise the efficiency typically start by maximising $\tau\alpha$ and minimising U_L. Heat loss coefficients $U_L \approx 3.8$ W/m^2 K are possible using a selective emissivity absorber coating to minimise

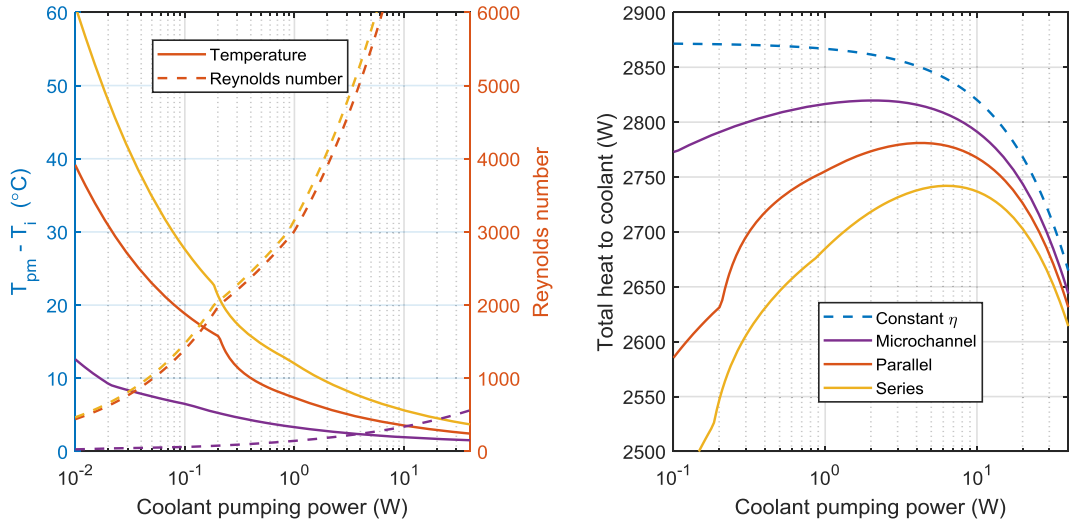

Fig. 1. Effect of varying pumping power on $\Delta T = T_{pm} - T_i$ and on overall heat flux to coolant. At low flow rates the increased plate mean temperature T_{pm} leads to increased heat loss and lower efficiency.

Table 2
Predicted optimum flow parameters for three PV-powered thermal collector systems.

	Parallel	Series	Microchannel plate
Modelled as:	Pair of 1 m wide × 2 m long panels in parallel	Pair of 1 m wide × 2 m long panels in series	6 mm square passages over 1 m width at 8 mm pitch; H = 4 m
Mass flow rate (kg/s)	0.115	0.0703	0.199
Mass flow rate (kg/m^2 s)	0.0288	0.0176	0.0498
Coolant pumping power (W)	4.21	6.39	1.99
• internal loss (W)	3.77	6.27	0.0396
• external loss (W)	0.442	0.118	1.95
Absorber W_p (W/m^2)	0.943	1.57	0.0099
$\Delta T = T_{pm} - T_i$ (°C)	4.60	6.48	2.78
PV area (m^2)	0.0421	0.0639	0.0199
Heat output (W), including electrical power	2781	2742	2820
Overall efficiency	0.6952	0.6855	0.7049

heat losses. The Tinox® Energy, for instance, combines $\tau > 0.95$ with $\varepsilon < 0.04$. A further measure is to employ a high vacuum to eliminate gaseous conduction: a number of manufacturers (Gensys, SRB, TVP) have been developing evacuated panels. If the internal pressure is reduced below 0.2 Pa, conduction losses are negligible and $U_L \approx 1$ W/m^2 K is possible. In-service heat loss coefficients may be higher due to scaling e.g. 5–6 W/m^2 K (Arunachala et al., 2015).

A further efficiency benefit may be obtained by careful choice of the coolant passage dimensions to minimise the difference between the mean plate temperature T_{pm} and the fluid inlet temperature T_i. To this end the design should ideally:

- use a high flow rate, such that the fluid temperature rise is small;
- minimise the spacing between flow channels and use a thick plate made of high conductivity material, such that the plate temperature varies little in the transverse direction;
- minimise the channel hydraulic diameter to provide high heat transfer coefficients.

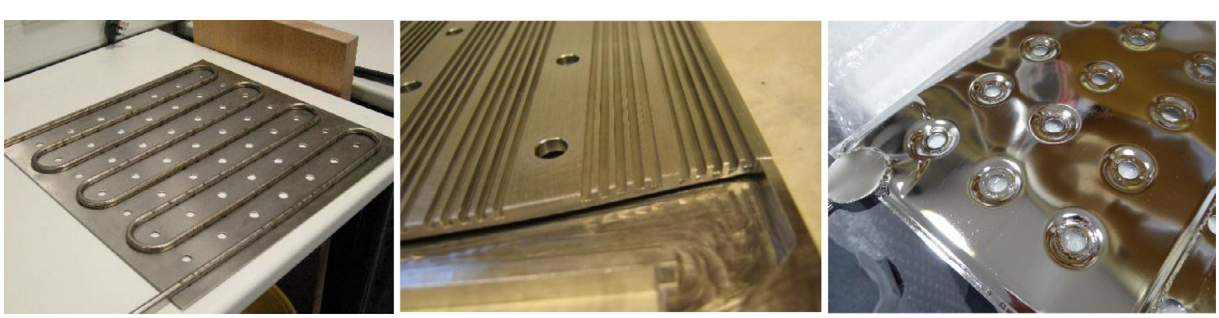

Fig. 2. Examples of the three kinds of solar absorber. (a) Serpentine tube on plate, (b) microchannel, prior to adding top cover, and (c) flooded panel. Experimental details and results will be reported elsewhere.

In some installations using stratified hot water tanks it has been found to be beneficial (Duffie & Beckman) to use a very low flow rate that results in a high coolant temperature rise across the panel, even though the panel efficiency can be reduced as a result. They distinguish between these "low flow" cases ($0.002 - 0.006\ \mathrm{kg/m^2\ s}$) and the more usual "mixed out" tank assumption with heat being passed to a constant temperature heat sink and typical mass flow rates $\approx 0.015\ \mathrm{kg/m^2\ s}$. The following analysis in terms of T_{pm} assumes a mixed out system where there is no advantage to be obtained from a high fluid temperature rise.

3.2. Calculation of pumping power

3.2.1. Geometrical definitions for microchannel passages

The cross-section for a microchannel will depend on the manufacturing process and might be circular, rectangular or some other section.

For calculation purposes the absorber is considered to be equivalent to a virtual microchannel plate with N circular passages of hydraulic diameter D_h (Fig. 3). It is assumed that the passage spacing is small enough and conductivity sufficiently high that lateral temperature variations between passages have no influence on the optimisation process: this means that the equations need not include metal thickness and conductivity terms. A more detailed analysis including conduction effects is presented in Section 3.6.

A microchannel system can be designed by first identifying a suitable hydraulic diameter and number of circular holes and then considering the equivalent dimensions and number of channels for any desired non-circular cross-section. The circular hole assumption will model the pressure drop and fluid-to-metal temperature difference correctly provided the friction coefficient f and Nusselt number Nu_H are appropriate for the actual channel cross-section.

A microchannel plate might use rectangular passages (Fig. 3b) but other profiles are possible e.g. with a hydro-formed or roll bonded plate (Del Col et al., 2013; Sun et al., 2014). The limiting case of flow between two parallel plates is discussed later as an extension of the microchannel analysis.

For rectangular passages the aspect ratio s is defined such that $a = sb$, giving $D_h = \frac{2ab}{a+b} = \frac{2sb}{(s+1)}$ (Table 3). Rearranging these as $b = \frac{(s+1)D_h}{2s}, a = \frac{(s+1)D_h}{2}$ allows an optimum hydraulic diameter to be converted back to equivalent rectangular channel dimensions. In the limiting case of a collector constructed from two parallel sheets at some spacing b the aspect ratio is infinite. In this case the hydraulic diameter is given by $D_h = 2b$.

When optimising the passage diameter it is assumed that the void fraction R is constant; it should in general be as high as mechanical strength considerations will allow. This geometric similarity constraint is essential for the optimisation process as well as being a logical design feature. Conversely if the passage pitch were held constant the best configuration would simply be to use the largest possible passages that could fit within the chosen pitch: it would not be optimum in terms of balancing the two temperature difference effects.

Table 3
Algebraic form of microchannel geometric parameters from Figs. 3(b) for the example where rectangular passages are modelled as circular holes. The passage length L = plate length H for a single-pass microchannel system.

	Rectangular passages	Equivalent circular holes
Dimensional definitions:	Channel dimensions $a \times b$, $s = \frac{a}{b}$	Diameter $D_h = \frac{2ab}{a+b} = \frac{2sb}{(s+1)}$
Number of holes across width W of the absorber	$n = \frac{W}{p}$	$N = \frac{n}{K} = \frac{RW}{D_h}$ where $K = \frac{\pi s}{(s+1)^2}$
Void fraction (diameter to pitch ratio)	$r = \frac{a}{p}$	$R = \frac{ND_h}{W} = r(\frac{D_h}{aK})$, pitch $P = \frac{D_h}{R}$

A typical design might use square channels ($s = 1$) at a 1:1 channel: rib ratio ($r = 0.5$), resulting in a circular equivalent centreline void fraction $R = \frac{2}{\pi} \approx 0.637$. A circular hole design must use $R < 1$ for mechanical strength reasons: in the limit at $R = 1$ the tubes would need zero wall thickness. Similarly in a microchannel plate the passages would merge at $R = 1$ (circular) or $r = 1$ (rectangular), leaving no mechanical attachment between top and bottom of the plate. A sensible void fraction value may depend on ease of fabrication as well as mechanical strength concerns. Serpentine tube absorbers will similarly be constrained to a limiting R value, approximately R < 0.2, due to the minimum possible bend radius.

3.2.2. Friction and flow rate calculations

The formulae for friction factor and Nusselt number in laminar flow are algebraically simple and lead to straightforward solutions for mean absorber temperature and optimum diameter that are useful when comparing single and double-pass systems.

The equivalent correlations for turbulent flow are more complex and require numerical solution. The laminar calculations are derived below, to illustrate the methodology and the definition of the parameters; results in the turbulent regime will however be presented without showing details of the Matlab calculations.

The pumping power per unit plate area is:

$$W_p = \frac{\dot{Q}\Delta P}{L} \tag{1}$$

Microchannel absorbers are likely to operate with laminar flow (Re < 2100). The Fanning friction factor is then $f = \frac{\mathrm{Po}}{\mathrm{Re}_D}$ and the pressure drop along the channels will be:

$$\Delta P = 4f\left(\frac{L}{D_h}\right)\left(\frac{1}{2}\rho v^2\right) = 4\frac{\mathrm{Po}\mu}{\rho v D_h}\left(\frac{L}{D_h}\right)\left(\frac{1}{2}\rho v^2\right) = \frac{2\mathrm{Po}\mu L v}{D_h^2} \tag{2}$$

The friction factor and Nusselt number methods used for microchannel and serpentine tube calculations are summarised in Table 4.

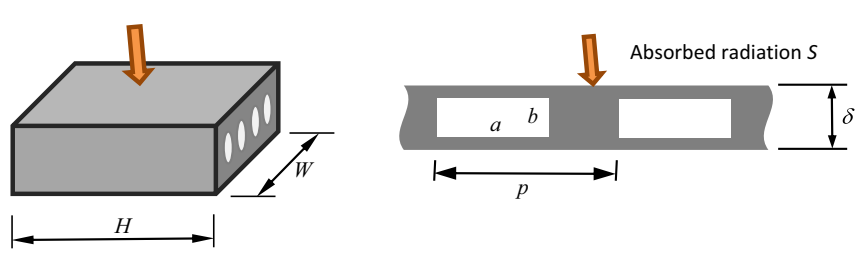

Fig. 3. (a) Virtual plate with circular channels and (b) nomenclature for a rectangular channel cross-section which may be modelled as an array of circular holes of equivalent area and perimeter. The passage side half-thickness t_s and top plate thickness t_t are defined as $p = a + 2t_s$, $\delta = b + 2t_t$.

Table 4
Formulae for friction factor and Nusselt number used in the simulations (Lorenzini and Morini, 2009; Massey, 1989; Kakac et al., 1987); Petukhov and Gnielinski correlations. Linear interpolation was used between the Re = 2000 and 3000 values in the transition region.

	Cross-section	Fanning friction factor f	Nusselt number
Laminar, Re < 2000 $f = \frac{\mathrm{Po}}{\mathrm{Re}_D}$	Circular	Po = 16	$\mathrm{Nu_H} = 4.36$
	Square	Po = 14.226	$\mathrm{Nu_H} = 3.612$
	Infinite parallel plates	Po = 24	• $Nu_H = \frac{140}{17} \approx 8.235$ (equal heat flux to each plate) • Heating top plate only $Nu_1 = \frac{140}{26} \approx 5.385$, $Nu_2 = 0$, $Nu_H = \frac{Nu_1+Nu_2}{2} = 2.692$
Turbulent, Re > 3000	Circular	$f = \frac{0.25}{(0.79 \ln \mathrm{Re} - 1.64)^2}$	$Nu_D = \frac{(\frac{f}{2})(\mathrm{Re}-1000)\mathrm{Pr}}{1+12.7\sqrt{\frac{f}{2}}(\mathrm{Pr}^{\frac{2}{3}}-1)}$

Combining Eqs. (1) and (2) the mass flow rate for laminar flow is:

$$\dot{m} = \rho\dot{Q} = \rho N\left(\frac{D_h^2}{4}\right)\sqrt{\frac{2\pi D_h W_p}{\mathrm{Po}\mu R}} \quad (\mathrm{kg/s}) \tag{3}$$

At higher Reynolds numbers the mass flow at each pumping power was determined numerically.

3.2.3. Extension to a parallel plate geometry

A parallel plate geometry is the limiting case of microchannels with an infinite aspect ratio. Defining a plate spacing b, the hydraulic diameter will be $D_h = 2b$. The equivalent number of passages must satisfy $2W = N\pi D_h$ to achieve the desired perimeter, hence $R = \frac{ND_h}{W} = \frac{2}{\pi}$.

Parallel plates and square section microchannels with 1:1 rib/channel widths therefore have the same R value and, with appropriate Nusselt and Poiseuille numbers, the same analysis may be used for both.

3.3. Heat transfer to fluid

3.3.1. Theory

The purpose of a solar collector is to take fluid, at some inlet temperature that is constrained by the system being heated, and deliver as much heat as possible to that fluid. The difference between the fluid inlet temperature and the mean plate temperature, $\Delta T = T_{pm} - T_i$, makes the plate "hotter than it needs to be", increasing thermal losses and reducing the net heat collected. The design aim is to minimise ΔT for a given pumping power.

For fully developed laminar flow with a constant heat flux boundary condition, the Nusselt number is expected to be a constant, Nu_H. Nusselt numbers vary slightly depending on the aspect ratio and thermal boundary condition, Table 4. For flooded panel absorbers the heat flux may be higher on the upper surface: the limiting cases are given for a panel with very good thermal contact between surfaces and for one with heat flux through the top surface only. The latter case might occur if using a material with poor thermal conductivity (steel or plastic as opposed to copper or aluminium). It has been assumed that flow passages are long enough for the mean Nusselt number to be unaffected by entry length effects.

ΔT has two components: the mean temperature rise of the fluid along the channels plus the fluid-to-metal temperature difference (inversely proportional to heat transfer coefficient h):

$$\Delta T = \bar{\theta} + \Delta T_h \tag{4}$$

For a single-pass configuration $\bar{\theta} = (\frac{T_o - T_i}{2})$. All fluid temperatures here refer to the mass-weighted mean temperature over the cross-section.

The net heat input to the plate Q_u will for simplicity be treated as a constant here since a good fluid flow design will achieve small ΔT and a heat removal rate very close to the maximum possible. The assumption is that the plate temperature is sufficiently uniform that local variations in heat loss $U_L(T(x) - T_a)$ are a small fraction of the net heat absorbed per unit area Q_u; this simplifies the analysis considerably.

This assumption may be justified in terms of an uncooled stagnation temperature difference $\Delta T_{\max} = \frac{G_T\tau\alpha}{U_L}$. The mean plate temperature from a constant heat input solution will be close to the exact solution provided $T_o - T_i < 0.2\Delta T_{\max}$ (or $\bar{\theta} < 0.1\Delta T_{\max}$). As an example, taking $G_T\tau\alpha = 800\ \mathrm{W/m^2}$ and $U_L = 4\ \mathrm{W/m^2K}$ gives $\Delta T_{\max} = 200\ ^\circ\mathrm{C}$; it is likely that any optimised system will achieve $T_o - T_i < 20\ ^\circ\mathrm{C}$ unless the pumping power is extremely low.

Both components of ΔT in Eq. (4) are proportional to the rate of heat extraction Q_u:

$$T_o - T_i = \frac{Q_u}{\dot{m}c} \text{ and } \Delta T_h = \frac{Q_u}{A_h h}$$

The net heat absorbed per unit area, S^*, is defined by:

$$Q_u = A_c[G\tau\alpha - U_L(T_{pm} - T_a)] = A_c S^*$$

Defining $\bar{\theta}$ and ΔT_h in terms of the pumping power (per unit collector area) W_p:

$$\bar{\theta} = \frac{(T_o - T_i)}{2} = \frac{A_c S^*}{2\dot{m}c} = \frac{WHS^*}{2}\left[\left(\frac{\rho c N D_h^{2.5}}{4}\right)\sqrt{\frac{2\pi W_p}{\mathrm{Po}\mu R}}\right]^{-1}$$

$$\Delta T_h = \frac{A_c S^*}{A_h h} = \frac{A_c S^*}{(LN\pi D_h)}\left(\frac{D_h}{kNu_H}\right) = S^*\left(\frac{D_h}{\pi k Nu_H R}\right)$$

Substituting the microchannel definitions $L = H$, $N = \frac{RW}{D_h}$ into Eq. (4):

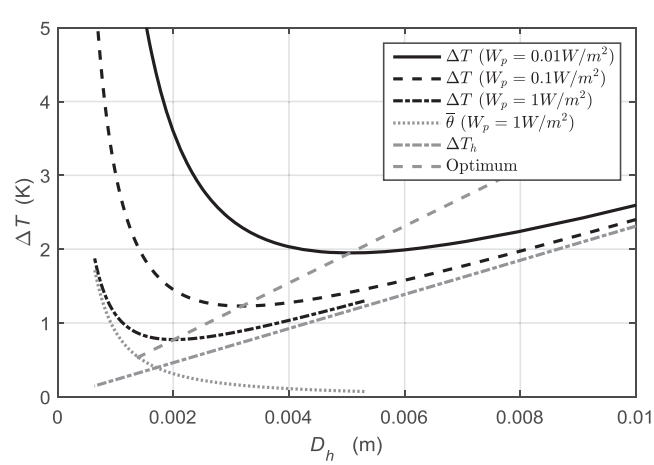

Fig. 4. Difference in temperature ΔT between fluid inlet and mean plate surface as a function of channel hydraulic diameter. This difference is the sum of a mean fluid temperature rise ΔT_{fm} and the temperature difference necessary by virtue of the finite heat transfer coefficient, ΔT_h. (Fluid is Tyfocor-LS at 70 °C, S^* = 750 W/m^2, square microchannels, H = 1 m, R = 0.637.)

$$\Delta T = S^*\left[\left(\frac{2H}{\rho c}\right)\sqrt{\frac{\mathrm{Po}\mu}{2\pi R W_p}}D_h^{-1.5} + \left(\frac{1}{\pi k Nu_H R}\right)D_h\right] \quad (5)$$

3.3.2. Heat transfer discussion

Reducing the channel size will reduce ΔT_h (because the heat transfer coefficient increases) but, for a constant W_P, reduce the mass flow rate and increase $\bar{\theta}$. The constraint that R is constant sets a constant internal passage surface area regardless of the diameter. For any chosen L, R and W_P there will be an optimum D_h for a given fluid that balances these two effects to minimise $\Delta T = T_{pm} - T_i$ (Fig. 4).

Fig. 4 shows that optimal values of microchannel hydraulic diameter lie in the range 2–6 mm for Tyfocor-LS at 70 °C with square-section channels.

ΔT graphs for a parallel plate collector (Fig. 5) are equivalent to a microchannel design but modelled with hydraulic diameter $D_h = 2b$.

Solar collectors are illuminated from one side only and the performance of a flooded panel, modelled as two parallel plates, will depend on the degree of thermal contact between the front and back plates. The microchannel analysis assumed that there was an effective thermal conduction path through the ribs: this is not necessarily true in the limiting case with two plates. Fig. 5 compares the two extremes of a single-sided and a double-sided analysis.

The dotted curves in Fig. 5 would be obtained from the microchannel results in Fig. 4 by the transformation $b = \frac{D_h}{2}$ if the Nusselt and Poiseulle numbers were invariant. Fig. 5 however uses the Nusselt and Poiseulle numbers for infinite parallel plates; both ΔT and the optimum spacing b are therefore slightly higher than would be expected from the square-section microchannel graph.

Eq. (5) also defines the effect of varying the channel void fraction R. If D_h is held constant, Eq. (5) may be simplified as $\frac{\Delta T}{S^*} = \frac{A_1}{\sqrt{R}} + \frac{A_2}{R}$, indicating that ΔT decreases as R increases. For a given hydraulic diameter, the best design will use the largest practicable value for R.

The optimum microchannel diameter, corresponding to the minima of the curves in Figs. 4 and 5, can be calculated by differentiating Eq. (5) with respect to D_h, subject to constant H and R, to give:

$$D_{h,opt} = \left[\frac{3kNu_H}{\rho c}\sqrt{\frac{\mathrm{Po}\pi\mu R H^2}{2W_p}}\right]^{0.4} \quad (6)$$

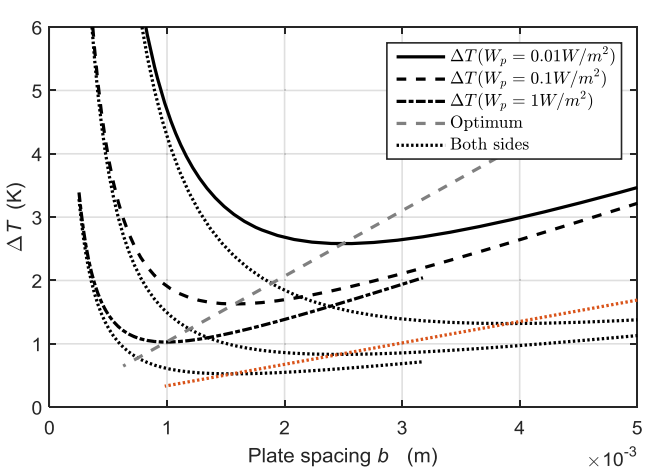

Fig. 5. Comparison of ΔT curves for a parallel plate collector when the fluid extracts heat from just one surface (bold) or both surfaces (dotted equivalents). (Fluid is Tyfocor-LS at 70 °C, S^* = 750 W/m^2, L = 1 m.)

If this condition is satisfied $\Delta T_{opt} \propto D_{h,opt}$ (resulting in the straight "Optimum" lines in Figs. 4 and 5) and $\Delta T \propto W_p^{-0.2}$ (since $D_{h,opt} \propto W_p^{-0.2}$); if R can also vary, $D_{h,opt} \propto R^{0.2}$ and then $\Delta T_{opt} \propto R^{-0.8}$.

The optimum hydraulic diameter increases with plate height H unless there is a corresponding increase in the pumping power per unit area W_p.

3.3.3. Effects due to absorber size

Figs. 4 and 5 have been plotted for a nominal height H = 1 m. An optimal design at one size would need scaling for use in a larger panel.

The mean fluid temperature rise $\bar{\theta}$ is proportional to $\sqrt{\frac{H^2}{W_p}}$ (microchannel case) because of the modelling assumption that S^* is constant; in practice if W_p/H^2 were very small, the fluid temperature would asymptote towards the plate stagnation temperature. The effect is not significant here because an optimised design will maintain the plate well below its stagnation temperature.

ΔT can be reduced by choosing a design with small H, for instance a rectangular plate could have the channels running across the plate rather than along it. This is similar to the concept of connecting multiple solar collectors in parallel rather than in series; it maximises the total channel cross-section area as well as minimising the channel length, thereby (for some total mass flow rate) reducing the fluid velocity and pressure drop. In practice however the design of inlet manifolds to achieve uniform flow partition between channels is likely to be easier with large H and small W than vice versa.

Similar values for ΔT can be achieved over a range of designs of differing size by selecting $W_p \propto H^2$. If this condition is satisfied $D_{h,opt}$ will be constant irrespective of the panel dimensions. Conversely if the pumping power per unit area W_p is kept constant the fluid temperature rise $\bar{\theta}$ will be proportional to plate length H and $D_{h,opt} \propto H^{0.4}$.

3.4. Fluid property effects

The fluid properties slightly influence the optimum hydraulic diameter for a given pumping power, Fig. 6.

Optimum D_h for a given pumping power is only a weak function of thermal diffusivity and viscosity so the variation in D_h is modest. The combination of higher viscosity and changes in thermal diffu-

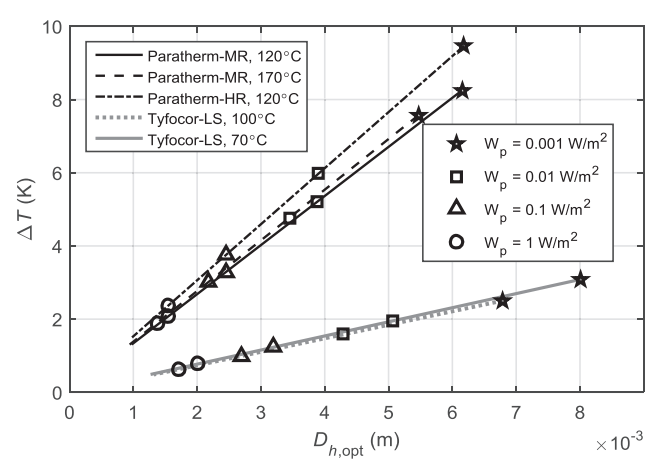

Fig. 6. Optimum microchannel hydraulic diameter, at various pumping powers (L = 1 m), for different liquids and temperatures. The higher viscosity fluid (Paratherm) requires a higher pumping power than Tyfocor to achieve the same ΔT. [Square channels, constant R (any fixed value).]

sivity does however result in the Paratherm simulations having higher ΔT unless the pumping power is increased considerably.

The Po and Nu_H values used here assume laminar flow, Re < 2000. This is unlikely to be exceeded in a microchannel plate: if necessary, though, a numerical method (Section 3.6) can be used to model the pressure drop and heat transfer at higher Reynolds numbers.

Practical considerations such as ease of manufacture or the size of manifolds and pipework necessary to ensure uniform flow distribution between channels may dictate the use of slightly smaller or larger hydraulic diameters. The temperature curves in Figs. 4 and 5 have broad minima so this can be accomplished with little loss of performance.

3.5. Comparison of single and double-pass microchannel systems

The preceding calculations have assumed that the mean fluid temperature is the mean of the inlet and outlet temperatures. This will be true for a single-pass microchannel system with uniform heat flux per unit area.

An alternative to the single pass concept would be a double-pass design with the microchannel plate folding back under itself. This appears attractive from an installation perspective, Fig. 7, because the manifolds and pipework could then connect to just one end of the collector.

A double-pass system could be implemented either as two stacked layers of channels, Fig. 7(b) or as interleaved channels, 7 (c). The stacked implementation allows a higher void fraction R which is beneficial because of the higher flow rate at any given pumping power and hydraulic diameter.

This folded configuration, assuming perfect thermal contact between forwards and return flow channels, resembles a serpentine-flow absorber with a single kink. The general case with multiple passes and both axial and lateral temperature variations is complex (Abdel-Khalik, 1976; Zhang and Lavan, 1985; Akgun, 1988; Lund, 1989); more recently Ho et al. (2007) performed a 2D analysis of the temperature distribution in a double-pass counter-flow heat exchanger with uniform heat flux to both external walls.

The double pass configuration is more common in solar air heaters than liquid-cooled absorbers (Chamoli et al., 2012). The temperature variation along double-pass air heater channels has been extensively modelled (Sopian et al., 1996; Othman et al., 2006; El-Sebaii et al., 2011; Hernández and Quiñonez, 2013). These models recognise the substantial temperature variations that may occur with air as the working fluid and the resulting axial variation in heat loss; the solution of the linked first-order equations uses a pair of exponential terms.

A much simpler expression for temperatures in a liquid-cooled double pass system is possible (Appendix A) since it is easier with water to ensure a sufficient flow rate that the range of $T(x)$ is much smaller than $\Delta T_{\max}$. It will be assumed as before that the net heat input is approximately constant over the plate and also that in the microchannel case with high metal conductivity and close channel spacing the only significant temperature gradients occur parallel with the flow direction. This simplifies the second–order equations to give a quadratic expression for each temperature: this approximation to the exact exponential form is analogous to the structural mechanics approximation of a catenary as a parabola.

The resulting graphs of plate surface and coolant temperature in the flow and return directions (Fig. 8) show that the fluid temperatures may be higher within the collector than at the outlet.

Both analyses here are for a sufficiently long, thin plate that axial heat conduction through the metal may be omitted from the model. Oyinlola et al. (2015a–2015c) presents a more detailed analysis showing the effects of axial conduction on the single-pass case.

At low flow rates, Fig. 8(b), heat transfer between liquid in the forward and reverse channels leads to a regenerator effect that increases the temperature difference between the manifold and the opposite ends of the plate. The mean fluid temperature may then be considerably higher than the fluid outlet temperature leading to an increased heat loss through radiation and conduction. This effect is minimised by increasing the flow rate; the optimum hydraulic diameter for a double-pass system is typically larger than in the equivalent single-pass system, Table 5. The effect is in accordance with the findings of Zhang and Lavan (1985) that the difference in F_R between the $N = 1$ and the $N = 2$ serpentine case is highest at low flow rates.

When comparing single and double-pass systems it is important to distinguish between double-pass systems having the same number of inlet channels as the datum single-pass case, Fig. 7(b) "stacked", and those having half as many, 7(c) "interleaved". The general shape of the curves of mean temperature against D_h for a double-pass systems closely resembles the single pass equivalent in Fig. 4. The optimum hydraulic diameter for a laminar flow double pass system is:

$$D_{h,opt} = \left(\left(3 + \sqrt{\frac{91}{3}}\right)\sqrt{\frac{\pi \mathrm{Po}\mu H^2}{RW_p}}\frac{Nu_H kR}{\rho c}\right)^{0.4}$$

The optimum double-pass parameters are simply a scaled version of the single pass equivalent. For any particular fluid properties, plate length and pumping power W_p, the relationship between optimum values can be expressed relative to a datum "case 1" single pass system (Table 5).

The stacked double configuration (2) achieves lower ΔT than the datum single pass case (1) because it has twice as many channels; a single pass system (3) with the same number of channels (2) however performs even better. (4), (5) are equivalent to (1), (2) with a reduced number of channels hence higher ΔT_{opt}. The illustrations show a repeating section with the appropriate ratio of passage diameter $D_{h,opt}$ and void ratio R. Given the assumption that temperature gradients within the metal may be ignored (see more detailed investigation in Section 3.6 below), at any given void fraction R there is no difference in performance between the interleaved and stacked geometries. The double-pass illustrations (2), (5) in Table 5 could equally well show the interleaved case. The stacked case does however allow the use of a higher R value which would increase efficiency and reduce ΔT.

All dimensions are relative to an optimum diameter from equation (6) for reference case (1).

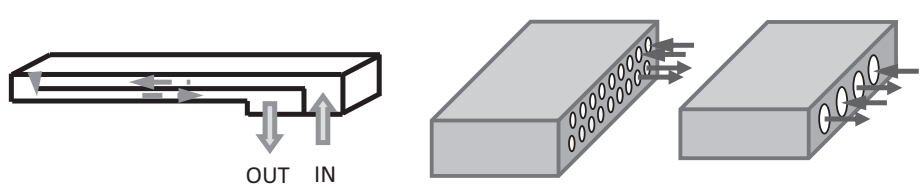

Fig. 7. (a) Possible configuration of a double-pass microchannel plate, (b) stacked, and (c) interleaved channel geometries for a double-pass system.

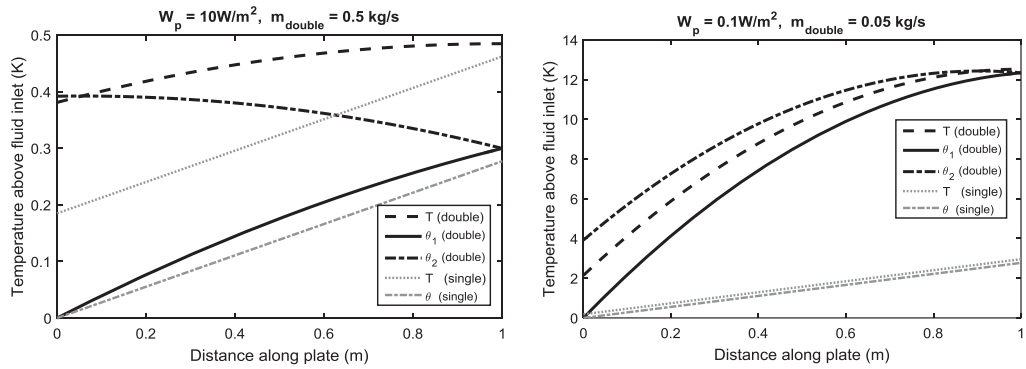

Fig. 8. Metal (T) and fluid (θ) temperature distributions along single and double-pass microchannel plates (a) high flow rate and (b) low flow rate. Square channels, R = 0.637, D_h = 1.6 mm, plate height = 1 m, Tyfocor-LS, S^* = 750 W/m^2, equivalent to one layer and two layers of the stacked design, Fig. 7(b).

Table 5
Relationships between optimum values for single and double pass laminar flow systems as a function of the void ratio R. The double-pass systems (2, 5) have been drawn as a stacked design for ease of comparison but could equally well be interleaved, albeit with limitations on the maximum R value. R is defined in terms of the pitch of passages flowing in parallel (Appendix A).

	Comparative geometry (to scale)	Optimum diameter ratio	Optimum temperature ratio
1) Single pass reference case , $R = R_1$	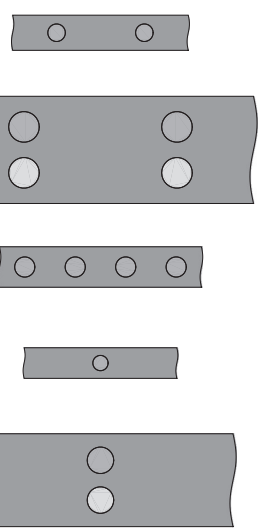	$D_{h,\text{opt},1}$	$\Delta T_{\text{opt},1}$
(2) Double, $R = R_1$		$D_{h,\text{opt},2} = 1.743 D_{h,\text{opt},1}$	$\Delta T_{\text{opt},2} = 0.807 \Delta T_{\text{opt},1}$
(3) Single pass, $R = 2R_1$		$D_{h,\text{opt},3} = 2^{0.2} D_{h,\text{opt},1} = 1.15 D_{h,\text{opt},1}$	$\Delta T_{\text{opt},3} = 2^{-0.8} \Delta T_{\text{opt},1} = 0.57 \Delta T_{\text{opt},1}$
(4) Single pass, $R = 0.5R_1$		$D_{h,\text{opt},4} = 0.5^{0.2} D_{h,\text{opt},1} = 0.87 D_{h,\text{opt},1}$	$\Delta T_{\text{opt},4} = 0.5^{-0.8} \Delta T_{\text{opt},1} = 1.74 \Delta T_{\text{opt},1}$
(5) Double, $R = 0.5R_1$		$D_{h,\text{opt},5} = 1.743 D_{h,\text{opt},4} = 1.51 D_{h,\text{opt},1}$	$\Delta T_{\text{opt},5} = 0.807 \Delta T_{\text{opt},4} = 1.40 \Delta T_{\text{opt},1}$

A double-pass microchannel system is more complex to manufacture than the single-pass equivalent and there is a small performance penalty. The double-pass system's convenience in having both inlet and outlet connections at one end of the absorber may however outweigh these considerations for some applications.

3.6. Characterisation of a microchannel plate in terms of heat removal factors

Duffie and Beckman (2013) define the collector heat removal factor F_R as the ratio of actual heat extracted to the heat that could be extracted, were the entire plate at the fluid inlet temperature. The plate efficiency formula then takes the form:

$$\eta = F_R\left[(\tau\alpha) - \frac{U_L(T_i - T_a)}{G}\right]$$

The heat removal factor is the product of a collector efficiency factor F' and a heat capacity factor F'':

$$F_R = F'F'' \tag{7}$$

where $F'' = m^*\left(1 - e^{-\frac{1}{m^*}}\right)$ and $m^* = \frac{\dot{m}c}{A_c U_L F'}$ for a single-pass system.

The optimum D_h can therefore be found by maximising F_R as opposed to minimising ΔT: this method does not rely on the assumption that S^* is constant.

The collector efficiency factor F' describes the ratio of heat flux to fluid between the actual collector flux q'_u and the ideal collector equivalent: $F' = \frac{q'_u}{G\tau\alpha - U_L(T_f - T_a)}$. F' is a non-dimensional measure of the mean difference between fluid (T_f) and plate surface temperatures; it is independent of $G\tau\alpha, T_f$ and T_a.

F' can be determined from a solution of the temperature field around a passage, Fig. 9.

The microchannel collector efficiency factor F' may be characterised in terms of a passage efficiency factor F_P. For square passages at pitch p:

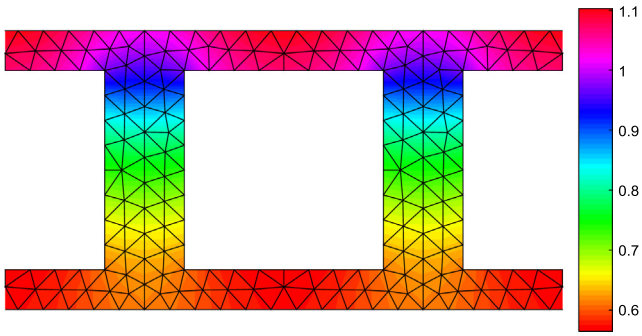

Fig. 9. Difference between metal and fluid temperature around a square-section microchannel passage made of stainless steel (k_m = 15 W/m K). $a = b = D_h$ = 5 mm, $p = \delta = 7$ mm ($t_t = t_s$), $G\tau\alpha = 870$ W/m^2, U_L = 3.8 W/m^2 K (top surface only), h = 320 W/m^2 K. $F' = 0.994$.

$$F' = \frac{\frac{1}{U_L}}{\frac{1}{U_L} + \frac{t_t}{k} + \frac{p}{F_P(4D_h h)}} \tag{8}$$

Material conductivity effects are only likely to be significant for large passage sizes and non-metallic materials. Such conditions could in theory occur in solar air heaters. For completeness, the passage efficiency factor F_P has been empirically correlated against numerical simulations over a wide range of conditions.

The correlation uses non-dimensional groups to model the wall thicknesses and conditions.

$$g_1 = \frac{t_s}{D_h}, \quad g_2 = \frac{ht_s}{k_m}, \quad G_1 = \frac{g_2}{g_1^2}, \quad G_2 = g_1 g_2$$

The "side" (to web mid-plane) and "top" thicknesses are defined as $p = a + 2t_s$, $\delta = b + 2t_t$ (Fig. 3). Two geometries were studied: $t_t = t_s$ and $t_t = 2t_s$.

$$F_{P1} = 0.25\Big(2 - 1.4\tanh(\log_{10}(0.83G_1)) - 0.5\tanh(\ln(0.35G_2^{0.6})) + 0.2e^{-\sqrt{G_2}} - 0.01\sqrt[4]{G_1} + 0.1\log_{10}g_1\Big)$$

$$F_{P2} = 0.25\Big(1.99 - 0.8\tanh(0.6\ln G_1 + 0.04) - 0.7\tanh(0.28\ln G_1 - 0.35) + 0.04e^{-0.1(\ln G_1+3)^2} + 0.02log_{10}g_1 - 0.49\tanh(\ln(0.5\sqrt{G_2})) + 0.09e^{-0.12(\ln G_2+0.79)^2}\Big)$$

(F_{P1}, F_{P2} for $t_t = t_s$ and $t_t = 2t_s$ respectively. Maximum F' error 0.0089, standard deviation 0.0017, for Biot numbers $\frac{hD_h}{k_m} \leqslant 400$. Each curve fit uses 7800 simulations covering $0.02 \leqslant G_4 \leqslant 0.5$, $0.5 \leqslant h_i \leqslant 800$ $0.01 \leqslant k \leqslant 200$ with $D_h = 0.005$, $U_L = 4$; correlations are independent of D_h and U_L. F_{P1} and F_{P2} are more similar than the equations might suggest: $\text{mean}\left(\frac{F_{P2}}{F_{P1}}\right) = 1.013$ and $1 \leqslant \frac{F_{P2}}{F_{P1}} \leqslant 1.23$ for comparisons with the same D_h, t_s, k_m, h values).

For a metal microchannel plate the thermal resistance is typically so low that any transverse variation in metal temperature has little effect on the overall efficiency. Setting $\frac{t_t}{k_m} \approx 0$, $F_P \approx 1$ allows Eq. (8) to be simplified as $F' \approx \left(1 + \frac{pU_L}{4D_h h_i}\right)^{-1}$ for a square passage and $F' \approx \left(1 + \frac{U_L}{\pi R h}\right)^{-1}$ for the circular hole equivalent.

Substituting $h = \frac{Nu_H k}{D_h}$, $F' \approx \left(1 + \frac{D_h U_L}{\pi k Nu_H R}\right)^{-1} = (1 + AD_h)^{-1}$ where $A = \frac{U_L}{\pi k Nu_H R}$

Fig. 10 shows equivalent curves to Fig. 4 plotted as heat recovery factor F_R rather than temperature difference and including transition to turbulent flow above Re > 2000. As before, if the plate size is increased or the pumping power is reduced then the optimum channel size will increase. Comparison of the Re/H curves for $W_{TOT} = 1000$ W and $W_{TOT} = 1$ W confirms that the scaling $W_{TOT} \propto H^3$, $W_p \propto H^2$ achieves constant mass flow/unit area whilst in the laminar flow regime; as expected, the corresponding F_R curves are identical until transition commences for the 1000 W curve at D_h = 0.001 m.

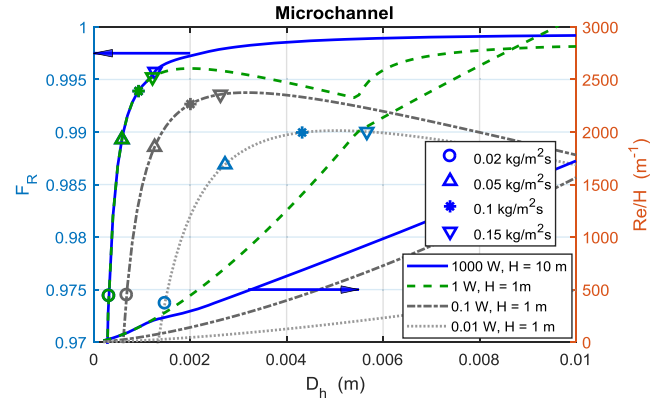

Fig. 10. Heat recovery factor F_R as a function of hydraulic diameter with U_L = 3.8 W/m^2 K. for a 1 m wide microchannel plate with square passages; R = 0.637, thickness $\delta = 1.5b$. The effects of transition commencing may be observed for the 1000 W and 1 W curves at D_h = 0.001 and 0.0053 m respectively. Aluminium plate, k = 222 W/m^2 K (F' = 0.994 at D_h = 0.005 m).

If sufficient pumping power is used to achieve turbulent flow the F_R curve rises monotonically with increasing hydraulic diameter and has no maximum (top curve in Fig. 10). This occurs because the increase in Nusselt number with Reynolds number in the turbulent regime offsets the fall in heat transfer coefficient that occurs in the laminar flow (constant Nu) case due to the $h = \frac{Nuk}{D_h}$ definition. This effect is however of little practical importance for microchannel solar collectors because high heat recovery factors can be achieved with much lower pumping powers under laminar conditions.

A satisfactory heat recovery factor of F_R = 0.99 is achieved for the 1 m^2 panel even with at the lowest pumping power of 0.01 W. The mass flow rate is then 0.124 kg/m^{2}s with an optimum hydraulic diameter of 5 mm.

Since the maxima are broad there is no need to determine the optimum D_h to great accuracy.

Substituting the metal plate approximation into Eq. (7), F_R can be defined in terms of D_h:

$$F_R = BD_h^{1.5}\left(1 - e^{-\frac{1}{m^*}}\right).$$

$$\text{with } m^* = \frac{\left(\frac{\rho c R W D_h^{1.5}}{4}\right)\sqrt{\frac{2\pi W_p}{\text{Po}\mu R}}}{WHU_L F'} = B(1 + AD_h)D_h^{1.5},$$

$$B = \left(\frac{\rho c R}{4U_L}\right)\sqrt{\frac{2\pi W_p}{\text{Po}\mu R H^2}}$$

This supports the conclusion from Section 3.3.3 that maintaining $W_p \propto H^2$ is necessary to avoid a reduction in efficiency as the plate length increases.

4. Analysis of serpentine tube systems

A serpentine tube system differs from a microchannel plate in that there is a single tube and its length is a function of plate width as well as length:

$$L = \frac{RWH}{D_h}, \quad N = 1.$$

The definition of length in terms of diameter to pitch ratio R assumes that the allowable bend radius is a multiple of pipe diameter i.e. the total pipe length must decrease if its diameter increases. It also assumes that the pitch and pipe length can be modelled as continuous variables whereas in practice the length will be close to an integer multiple of W or H. The approximation is acceptable provided the number of bends is large.

Eq. (7) has been used with the following tube on plate collector efficiency factor formulae (Duffie & Beckman):

$F = \frac{\tanh(m(W-D)/2)}{m(W-D)/2}$, $m = \sqrt{\frac{U_L}{k_m \delta}}$ with metal conductivity k_m and plate thickness δ.

$F' = \frac{1}{U_L P\left(\frac{1}{U_L(D+(P-D)F)} + \frac{1}{C_b} + \frac{1}{\pi D_h h}\right)}$ where tube outer diameter $D = D_h + 2\delta$, C_b is bond conductance and P is tube pitch.

A serpentine tube absorber is likely to have a smaller flow cross-sectional area than a microchannel plate and at similar mass flow rates the Reynolds number is higher. Serpentine tube systems typically operate in the turbulent regime, except for very small panels at low flow rates. When using Tyfocor at 70 °C the pumping power required to reach $\mathrm{Re} = 2000$ is approximately $W_p = 3.1 \times 10^{-7} \frac{R}{D_h^3}$ (W/m^2) i.e. 0.06 W/m^2 for an 8 mm bore tube with $R = 0.1$; higher powers will produce transitional or turbulent flow.

A serpentine tube may experience Reynolds numbers up to 50,000, Fig. 11(b). The Petukhov friction factor formula for turbulent flows (Table 1) may be approximated within 2.6% over the range $3000 < \mathrm{Re} < 50000$ as $f = 0.1001\mathrm{Re}^{-0.275}$. A constant mass flow per unit area will then be expected if $W_p \propto (WH)^{2.725}$.

The pumping power requirement can be reduced by connecting multiple panels in parallel rather than series; for instance, increasing the area of a 1 m wide panel by connecting W panels in parallel as opposed to widening a single panel would remove the W dependency, $W_p \propto (H)^{2.725}$.

Compared with a microchannel plate there will be an additional pressure drop due to flow around the pipe bends. Chen et al. (2003) provides correlations for pressure drop through multiple closely spaced bends over a wide Reynolds number range. Hassoon (1982) defines an "equivalent length" $\frac{L}{D} \approx 14$ at $\frac{r}{D} \approx 3$ (r = bend radius, equivalent to $R = \frac{1}{6}$) as a means of predicting the pressure drop for turbulent flow in a 180° bend. Hassoon's technique has been used for the numerical solutions in Figs. 11 and 12.

A tube on plate absorber suffers more from thermal resistance effects than a microchannel plate because the tube spacing is a much larger multiple of plate thickness. The simulations have been performed both for an infinitely thick plate ($F = 1$) and for a thin (0.9 mm) plate made of 1050 aluminium alloy, Fig. 11.

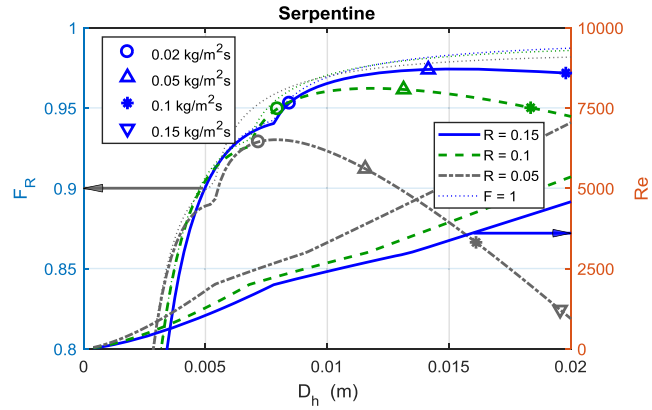

Fig. 12. Effect of varying the diameter to pitch ratio R. (W_{TOT} = 0.1 W, WH = 1 m^2).

The thick plate simulations of heat recovery factor F_R (dotted curves, $F = 1$) resemble the turbulent part of the microchannel curve in Fig. 10 and rise steadily as hydraulic diameter increases.

When the thermal resistance of a 0.9 mm thick plate is included the increased tube pitch at large D_h results in a decline in F_R. Each curve then has a broad maximum around the optimum hydraulic diameter with peaks at $F_R = 0.986$, 0.978, 0.962 occurring for $D_h = 7.4$, 9.2, 11.8 mm with mass flow rates of 0.084, 0.056 and 0.04 kg/m^{2}s respectively as the pumping power is varied between 10 W and 0.1 W. The variation of optimum F_R between the three curves is modest and as indicated in Section 2 the increase in pumping power may have a cost in terms of system economics.

It would be useful, given the importance of the pumping power, pitch, hydraulic diameter and mass flow rate, if these parameters were routinely measured and presented in papers on solar collector test results. This would provide some insight into whether efficiency differences between panels were the result of a superior design or simply a higher flow rate.

The mass flow markers indicate the range of flow rates commonly used in solar collectors (Duffie and Beckman). At any given flow rate, for instance the circular 0.02 kg/m^2 s markers, F_R rises if a smaller diameter tube and higher pumping power are used. Conversely at a given pumping power the maxima in the FR curves are very broad; changes in D_h that vary the mass flow rate in the range 0.05–0.1 kg/m^{2}s lead only to small changes in F_R, particularly at the highest pumping power (blue line in Fig. 11(a)).

Bend losses become relatively less important as the tube length between bends increases. For the simulations in Fig. 11(b), omitting the bend losses would raise the Reynolds number by 3.7, 2.7 and 1.9% respectively for the 1, 2 and 4 m^2 panels at the point with

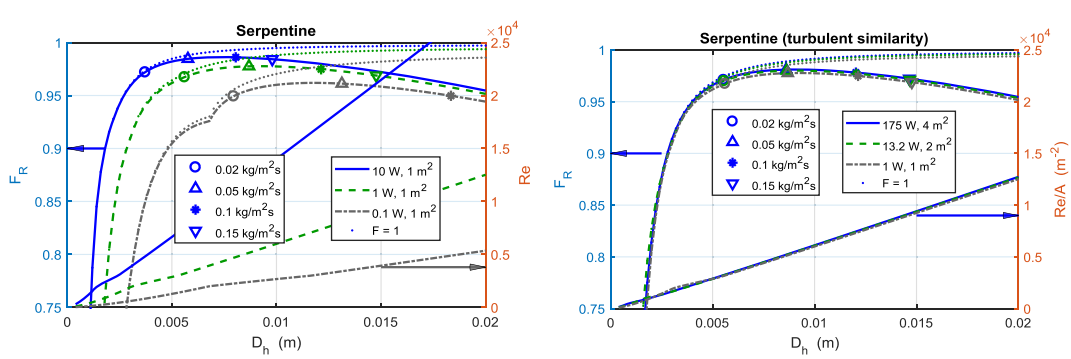

Fig. 11. Heat recovery factor F_R for a square aspect ratio ($W = H$) serpentine tube absorber, $R = 0.1$, with $U_L = 3.8$ W/m^2 K at various absolute pumping powers. Dotted lines show infinitely thick plate equivalent. (a) Effect of varying pumping power with constant panel area (b) $W_p \propto (WH)^{2.725}$, $W_{TOT} \propto (WH)^{3.725}$ for turbulent flow similarity as panel area varies. The highest Reynolds number is 51,000.

D_h = 0.008 m. Apart from changing the onset of transition, the effect on F_R is insignificant.

It has been assumed that a serpentine tube with multiple bends may be modelled in terms of the straight tube equations given above. The effect of conduction between adjacent tubes will be to slightly modify the relationship between fluid temperatures at inlet and outlet and the mean temperature. The effect with multiple passes is however likely to be much less severe than in the double-pass microchannel analysis in Section 3.5; for large N the heat removal factor is closer to the $N = 1$ than the $N = 2$ case (Zhang and Lavan, 1985). If the plate conductivity is so low that the tube sections are effectively isolated from each other, the system will behave like a single-pass design. The single-pass equation would also be an exact model if the conductivity were so high that axial conduction enforced a uniform temperature over the plate.

The tube length is proportional to the diameter: pitch ratio R. High R values (solid line in Fig. 12) increase the tube surface area and reduce the thermal resistance of the plate for a given D_h and pumping power; conversely they reduce the mass flow rate. For the parameters considered here the highest R value (0.15) achieves highest heat removal. For each curve, the optimum D_h rises with R giving $D_{h,opt}$ = 8, 11.8, 15.5 mm for R = 0.05, 0.1, 0.15 and tube pitch P = 160, 118, 103 mm respectively; higher pumping powers will have smaller optimum diameters.

The investigation into optimal system pumping power in Section 2 assumed a tube bore of 10 mm for the serpentine tube collectors. An iterative process can be used to identify a more suitable diameter. For instance, a similar graph to Fig. 11(a) with R = 0.15, 1.885 W, 2 m^2 would model the peak power point for the one branch of the parallel configuration in Table 2; the optimum diameter is 0.0144 m and, re-running the Table 2 simulation, the heat output would rise from 2781 to 2789 W. This is however still 1.1% below the heat obtained from the microchannel collector.

A similar graph with R = 0.15, 6.27 W, 4 m^2 would model the series case, giving an optimum diameter of 0.0162 m and raising the heat output by 1.2% i.e. from 2742 to 2775 W

5. Conclusions

The optimum channel or tube size for a flat plate collector will minimise heat losses, for some choice of diameter/pitch ratio and pumping power, by ensuring the mean absorber surface temperature is no higher than necessary.

The optimum pumping power can be determined by a simulation based on flow resistance around the installed system together with relative energy costs and collector efficiency characteristics. Both the optimum pumping power and passage hydraulic diameter have broad distributions and it is not essential for values to be determined to great accuracy. The pumping power requirement rises rapidly with tube or passage length; pumping power requirements may be minimised by connecting multiple solar collectors in parallel rather than in series. Optimal pumping powers for a 4 m^2 system were in the range 0.01 W/m^2 (microchannel) to 1.7 W/m^2 (serpentine).

Microchannel plates typically operate under laminar flow conditions. For a given pumping power an optimum diameter occurs because mass flow rate falls at small diameters and heat transfer coefficient falls at large diameters. The collector efficiency factor F' is typically higher than for a tube on plate absorber: this makes microchannel systems particularly suitable for designs using low conductivity materials such as stainless steel or a polymer. An empirical correlation for F' has been derived from finite element simulation results. The short conduction paths in a microchannel collector allow the use of low conductivity materials such as stainless steel or a polymer.

Optimal values of hydraulic diameter in a 1 m long microchannel plate lie in the range 2–5 mm for pumping powers between 1 and 0.1 W/m^2 when using Tyfocor-LS at 70 °C. Longer passages, lower pumping powers and more viscous fluids will require larger diameters.

Hydraulic diameters in this range can be achieved using a flooded panel collector in which two hydroformed sheets are welded together: there is no need for the very small hydraulic diameters that would only be possible via a microchannel design.

Double-pass microchannel plates have a larger optimum diameter and slightly lower thermal efficiency than the single pass equivalent.

Tube on plate absorbers typically operate under turbulent flow conditions. For a given pumping power and plate thickness an optimum diameter occurs because mass flow rate falls at small diameters and fin efficiency falls at large tube spacing. Optimum diameters were in the range 6–16 mm depending on pumping power and diameter/pitch ratio. Manufacturing constraints in terms of bend radius limit the maximum diameter/pitch ratio. Over the range of parameters investigated, the highest efficiency was obtained with the largest diameter/pitch ratio, R = 0.15. Larger ratios lead to reduced mass flow rates because the tube length increases; they are also unsatisfactory due to the tight bend radius required.

If the tube diameter is allowed to vary whilst keeping the pumping power and diameter/pitch ratio constant, there is very little variation in panel efficiency between mass flow rates of 0.05 and 0.1 kg/m^{2}s. For the cases investigated here, use of an excessively high pumping power reduced the effective heat output by 6%; lack of optimisation reduced it by 1% and the parallel-connected serpentine tube collectors produced 1.1% less heat than the microchannel design.

Papers publishing efficiency test results should provide details of the pumping power, pitch and hydraulic diameter to facilitate comparisons with other work.

Acknowledgements and Data Access

The authors are grateful to the Engineering and Physical Sciences Research Council (EPSRC) for funding this work as part of a collaborative programme between Warwick, Loughborough and Ulster universities, reference EP/K009915/1, EP/K010107/1 and EP/K009230/1. Matlab figures and code used in the production of this paper are openly available at http://wrap.warwick.ac.uk/88819.

Appendix A

A.1. 1-D analysis of flow temperatures in a two-pass microchannel system

The plate is assumed to be long and thin; axial conduction is not modelled.

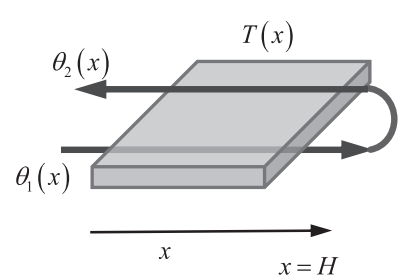

The channels are simulated as a colder "forwards" flow temperature $\theta_1(x)$, followed by a hotter "returning" flow temperature $\theta_2(x)$. Each cross-section of the plate has a constant metal temperature $T(x)$; it is assumed that temperature variations in the thickness and transverse directions may be neglected, together with axial conduction effects. $\theta_1(x), \theta_2(x) and T(x)$ are temperature differences relative to flow inlet i.e. $\theta_1(0) = 0$.

The mean of the two flow temperatures is: $\phi(x) = \frac{\theta_1(x)+\theta_2(x)}{2}$.

It is convenient to also define $\psi(x) = \frac{\theta_2(x)-\theta_1(x)}{2}$ such that $\theta_2(x) = \phi(x) + \psi(x)$ and $\theta_1(x) = \phi(x) - \psi(x)$

Over the width W there are N_P "cold" channels in parallel and a further N_P "hot" channels carrying return flow. Each has a hydraulic diameter D_h and an internal heat transfer coefficient h. The mass flow rate for the N_P cold holes is $\dot{m}$. The hole fraction R is defined in terms of N_P (as opposed to the total number of holes $2N_P$), $RW = N_p D_h$.

Heat transfer to the outbound and returning fluid, assuming a constant net heat flux S^* per unit area:

Over any short distance dx, $WS^*\mathrm{d}x = (N_P \pi D_h \mathrm{d}x)h[(T-\theta_1)+(T-\theta_2)]$

$$WS^* = (N_P \pi D_h h)[2T - (\theta_1+\theta_2)] = (2N_P \pi D_h h)[T-\phi] \tag{9}$$

Let $\alpha = \frac{N_P \pi D_h h_i}{\dot{m}c}$ such that $\frac{\mathrm{d}\theta_1}{\mathrm{d}x} = \alpha(T-\theta_1)$; similarly $\frac{\mathrm{d}\theta_2}{\mathrm{d}x} = -\alpha(T-\theta_2)$

Defining $M = \frac{\dot{m}c}{W}$, $\frac{\mathrm{d}^2\phi}{\mathrm{d}x^2} = -\frac{\pi h R S^*}{2M^2}$

Integrating and applying boundary conditions:

$$\theta_1(x) = \frac{S^*}{2M}\left(\frac{\pi R N u_H k}{M D_h}\left(-\frac{x^2}{2}+Hx\right)+(x-H)+H\right)$$

$$\theta_2(x) = \frac{S^*}{2M}\left(\frac{\pi R N u_H k}{M D_h}\left(-\frac{x^2}{2}+Hx\right)-(x-H)+H\right)$$

$$T(x) = \frac{S^*}{2M}\left[\frac{\pi R N u_H k}{M D_h}\left(-\frac{x^2}{2}+Hx\right)+H\right]+\frac{S^* D_h}{2\pi R N u_H k}$$

Alternatively if S^* were *not* assumed to be constant Eq. (9) would take the form $W(G\tau\alpha - U_L T) = (2N_P \pi D_h h)[T-\phi]$. Substitution into the linked equations $\frac{\mathrm{d}\theta_1}{\mathrm{d}x} = \alpha(T-\theta_1)$, $\frac{\mathrm{d}\theta_2}{\mathrm{d}x} = -\alpha(T-\theta_2)$ then produces an eigenvalue solution with exponential terms. The advantage of the quadratic solution given here is that it has simple expressions for the coefficients.

To find the mean fluid temperature $\bar{\phi}$ and plate temperature $\bar{T}$,

$$\bar{\phi} = \frac{1}{H}\int_0^H \phi \mathrm{d}x = \frac{HS^*}{2M}\left[\frac{\pi R N u_H k H}{3 M D_h}+1\right]$$

$\bar{\phi}$ can be used in place of the single-pass $\bar{\theta} = \frac{T_o - T_i}{2}$ to optimise a double-pass system.

Assuming laminar flow, adapting equations (1)–(3) for the longer overall channel length in a double pass system and neglecting any pressure drop at the 180° bend, the mass flow rate is:

$\dot{m} = \left(\frac{\rho W}{4}\right)\sqrt{\frac{\pi R W_p}{\mathrm{Po}\mu}} D_h^{1.5}$ i.e. $\frac{1}{\sqrt{2}}\times$ the single-pass mass flow for the given parameters. (The Poiseuille number could be raised to simulate bend pressure drop if necessary).

$$\bar{T} = \bar{\phi} + \Delta T_h$$
$$= S^*\left[\sqrt{\frac{\mathrm{Po}\mu H^2}{\pi R W_p}}\left(\frac{2}{\rho c D_h^{1.5}}\right)\left[\sqrt{\frac{\mathrm{Po}\mu H^2}{\pi R W_p}}\left(\frac{4\pi R N u_H k}{3\rho c D_h^{2.5}}\right)+1\right]+\left(\frac{1}{2\pi R N u_H k}\right)D_h\right]$$

References

Abdel-Khalik, S.I., 1976. Heat removal factor for a flat plate collector with a serpentine tube. Sol. Energy 18, 59–64.

Akgun, M.A., 1988. Heat removal factor for a serpentine absorber plate. Sol. Energy 41 (1), 109–111.

Agrawal, S., Tiwari, G.N., 2011. Energy and exergy analysis of hybrid microchannel photovoltaic thermal module. Sol. Energy 85, 356–370.

Arunachala, U.C., Bhatt, M.S., Sreepathi, L.K., 2015. Analytical and experimental investigation to determine the variation of Hottel-Whillier-Bliss constants for a scaled forced circulation flat-plate solar water heater. ASME J. Sol. Energy Eng. 137, 051011.

Aste, N., Del Pero, C., Leonforte, F., 2012. Optimization of solar thermal fraction in PVT systems. Energy Procedia 30, 8–18.

Bracamonte, J., Baritto, M., 2013. Optimal aspect ratios for non-isothermal flat plate solar collectors for air heating. Sol. Energy 97, 605–613.

Caffell, A., Low flow-rate pump, US patent 5,769,069, June 1998, retrieved from <https://patentimages.storage.googleapis.com/pdfs/US5769069.pdf>.

Cerón, J.F., Pérez-García, J., Solano, J.P., García, A., Herrero-Martín, R., 2015. A coupled numerical model for tube-on-sheet flat-plate solar liquid collectors. Analysis and validation of the heat transfer mechanisms. Appl. Energy 140, 275–287.

Chamoli, S., Chauhan, R., Thakur, N.S., Saini, J.S., 2012. A review of the performance of double pass solar air heater. Renew. Sustain. Energy Rev. 16, 481–492.

Chen, Z., Furbo, S., Perers, B., Fan, J., Andersen, E., 2012. Efficiencies of flat plate solar collectors at different flow rates. Energy Procedia 30, 65–67.

Chen, I.Y., Lai, Y.K., Wang, C.-C., 2003. Frictional performance of U-type wavy tubes. J. Fluids Eng. 125, 880–886.

Colangelo, G., Favale, E., Miglietta, P., de Risi, A., Milanese, M., Laforgia, D., 2015. Experimental test of an innovative high concentration nanofluid solar collector. Appl. Energy 154, 874–881.

Deng, Y., Zhao, Y., Wang, W., Quan, Z., Wang, L., Yu, D., 2013. Experimental investigation of performance for the novel flat plate solar collector with microchannel heat pipe array (MHPA-FPC). Appl. Therm. Energy 54, 440–449.

Del Col, D., Padovan, A., Bortolato, M., Pré, M.D., Zambolin, E., 2013. Thermal performance of flat plate solar collectors with sheet-and-tube and roll-bond absorbers. Energy 58 (September), 258–269.

Do Ango, M., Medale, M., Abid, C., 2013. Optimization of the design of a polymer flat plate solar collector. Sol. Energy 87, 64–75.

Dubey, S., Tiwari, G.N., 2009. Analysis of PV/T flat plate water collectors connected in series. Sol. Energy 83, 1485–1498.

Duffie, J.A., Beckman, A., 2013. Solar Engineering of Thermal Processes. Wiley.

Eisenmann, W., Vajen, K., Ackermann, H., 2004. On the correlations between collector efficiency factor and material content of parallel flow flat-plate solar collectors. Sol. Energy 76, 381–387.

El-Sebaii, A.A., Aboul-Enein, S., Ramadan, M.R.I., Shalaby, S.M., Moharram, B.M., 2011. Thermal performance investigation of double pass-finned plate solar air heater. Appl. Energy 88, 1727–1739.

Evola, G., Marletta, L., 2014. Exergy and thermoeconomic optimization of a water-cooled glazed hybrid photovoltaic/thermal (PVT) collector. Sol. Energy 107, 12–15.

Farahat, S., Sarhaddi, F., Ajam, H., 2009. Exergetic optimisation of flat plate solar collectors. Renew. Energy 34, 1169–1174.

Hassoon, H.M., 1982. Pressure drop in 180° bends. Build. Serv. Eng. Res. 3 (2), 70–74.

Hegazy, A.A., 1996. Optimization of flow-channel depth for conventional flat plate solar air heaters. Renew. Energy 7 (1), 15–21.

Hegazy, A.A., 1999. Optimizing the thermohydraulic performance of plate solar air heaters operating with variable pumping power. Renew. Energy 18, 283–304.

Henshall, P., Eames, P., Arya, F., Hyde, T., Moss, R., Shire, S., 2016. Constant temperature induced stresses in evacuated enclosures for high performance flat plate solar collectors. Sol. Energy 127, 250–261.

Hernández, A.L., Quiñonez, J.E., 2013. Analytical models of thermal performance of solar air heaters of double-parallel flow and double-pass counter flow. Renew. Energy 55, 380–391.

Ho, C.-D., Chuang, Y.-J., Tu, Y.-J., 2007. Double-pass flow heat transfer in a parallel-plate channel for improved device performance under uniform heat fluxes. Int. J. Heat Mass Transf. 50, 2208–2216.

Hussien, A.A., Abdullah, Mohd Z., Al-Nimr, Moh'd A., 2016. Single-phase heat transfer enhancement in micro/minichannels using nanofluids: theory and applications. Appl. Energy 164, 733–755.

Kakac, S., Shah, R.K., Aung, W., 1987. Handbook of Single-Phase Convective Heat Transfer. John Wiley & Sons.

Lorenzini, M., Morini, G.L., 2009. Poiseuille and Nusselt numbers for laminar flow in microchannels with rounded corners. In: 2nd Micro and Nano Flows Conference, London, September 2009 <http://bura.brunel.ac.uk/bitstream/2438/6936/1/MNF2009.pdf> (accessed 8/9/2015).

Lund, K. O'Ferrall, 1989. General thermal analysis of serpentine-flow flat plate solar collector absorbers. Sol. Energy 42 (2), 133–142.

Mansour, M.K., 2013. Thermal analysis of novel mini channel-based solar flat plate collector. Energy 60, 333–343.

Massey, B., 1989. Mechanics of Fluids. Chapman & Hall.

Nikoofard, S., Ugursal, V.I., Beausoleil-Morrison, I., 2014. An investigation of the technoeconomic feasibility of solar domestic hot water heating for the Canadian housing stock. Sol. Energy 101, 308–320.

Notton, G., Motte, F., Cristofari, C., Canaletti, J-L., 2014. Performances and numerical optimization of a novel thermal solar collector for residential building. Renew. Sustain. Energy Rev. 33, 60–73.
Othman, M.Y., Yatim, B., Sopian, K., Bakar, M.N.A., 2006. Double-pass photovoltaic-thermal solar collector. J. Energy Eng. 132 (3), 121–126.
Oyinlola, M.A., Shire, G.S.F., Moss, R.W., 2015a. The significance of scaling effects in a solar absorber plate with microchannels. Appl. Therm. Eng. 90 (2015), 499–508.
Oyinlola, M.A., Shire, G.S.F., Moss, R.W., 2015b. Investigating the effects of geometry in solar thermal absorber plates with microchannels. Int. J. Heat Mass Transf. 90 (2015), 552–560.
Oyinlola, M.A., Shire, G.S.F., Moss, R.W., 2015c. Thermal analysis of a solar collector absorber plate with microchannels. Exp. Therm. Fluid Sci. 67, 102–110.
Radwan, A., Ookawara, S., Ahmed, M., 2016. Analysis and simulation of concentrating photovoltaic systems with a microchannel heat sink. Sol. Energy 136, 35–48.
Roberts, D.E., 2013. A figure of merit for selective absorbers in flat plate solar water heaters. Sol. Energy 98, 503–510.
Sharma, N., Diaz, G., 2011. Performance model of a novel evacuated-tube solar collector based on minichannels. Sol. Energy 85, 881–890.
Sopian, K., Yigit, K.S., Liu, H.T., Kakaç, S., Veziroglu, T.N., 1996. Performance analysis of photovoltaic thermal air heaters. Energy Convers. Manage. 37 (11), 1657–1670.
Sun, X., Wu, J., Dai, Y., Wang, R., 2014. Experimental study on roll-bond collector/evaporator with optimized channel used in direct expansion solar assisted heat pump water heating system. Appl. Therm. Eng. 66, 571–579.
Visa, I., Duta, A., Comsit, M., Moldovan, M., Ciobanu, D., Saulescu, R., Burduhos, B., 2015. Design and experimental optimisation of a novel flat plate solar thermal collector for facades integration. Appl. Therm. Eng. 90, 432–443.
Xu, P., Shen, J., Zhang, X., He, W., Zhao, X., 2015. Design, fabrication and experimental study of a novel loop heat-pipe based solar thermal facade water heating system. Energy Procedia 75, 566–571.
Zhang, H.-F., Lavan, Z., 1985. Thermal performance of a serpentine absorber plate. Sol. Energy 34 (2), 175–177.